

FABRICATION AND CHARACTERIZATION OF SUGARCANE BAGASSE BASED CELLULOSE ACETATE/ZEOLITE (CA/Ze) MATERIAL FOR ELIMINATION OF Pb AND Cu IONS FROM AQUEOUS SOLUTIONS

TRANG THI CAM TRUONG,* NGA THI THUY DUONG** and HA MANH BUI***

*Faculty of Environment, University of Science, Viet Nam National University Ho Chi Minh City, Campus 1,
227 Nguyen Van Cu Str., Ward 4, District 5, Ho Chi Minh City 70000, Viet Nam

**Ho Chi Minh City University of Natural Resources and Environment, 236 Le Van Sy Str.,
Tan Binh District, Ho Chi Minh City 70000, Viet Nam

***Faculty of Environment, Saigon University, 273 An Duong Vuong Str., District 5,
Ho Chi Minh City 70000, Viet Nam

✉Corresponding author: H. Manh Bui, manhhakg@sgu.edu.vn

Received May 20, 2023

This study explores the synthesis and characterization of cellulose acetate/zeolite (CA/Ze) fibers as effective adsorbents for the removal of Pb^{2+} and Cu^{2+} ions from aqueous solutions. Cellulose acetate was derived from sugarcane bagasse (SCB) and integrated with zeolite to create CA/Ze fibers. Characterization techniques, including FTIR spectroscopy and SEM analyses, confirmed the successful modification and incorporation of zeolite within the fiber structure. Hydration studies revealed the fibers' stability in water, while adsorption experiments examined factors affecting adsorption capacity, such as pH, time, initial concentration, and reuse. The Langmuir and Freundlich isothermal models were applied to analyze adsorption isotherms. The results demonstrated the potential of CA/Ze fibers for efficient heavy metal removal, with a maximum adsorption capacity for Pb^{2+} ions of 13.9 mg/g. While the adsorption efficiency decreased after regeneration cycles, CA/Ze fibers displayed promise as sustainable adsorbents. This research contributes to addressing heavy metal pollution while promoting eco-friendly waste utilization.

Keywords: sugarcane bagasse, Pb^{2+} ion, Cu^{2+} ions, cellulose acetate/zeolite fibers

INTRODUCTION

Today, the escalating threat posed by heavy metal pollution originating from industrial activities looms ominously over both human well-being and ecological stability. This menace is underscored by the concurrent trends of increasing toxicity, sustainability concerns, and the alarming bioconcentration of heavy metals in natural habitats.^{1,2} In response to this perilous situation, the imperative for implementing effective treatment methods aimed at mitigating or eradicating heavy metal contamination in aquatic environments has never been more pronounced.

The quest for such treatment methods has engendered a multitude of investigations and innovations across various scientific disciplines. These endeavors have yielded a spectrum of

techniques for heavy metal removal, including chemical precipitation, ion exchange, electrochemical processes, biological methodologies, membrane-based approaches, and adsorption-based strategies.^{3,4} Among these methods, adsorption stands out as a particularly compelling option due to its inherent simplicity, ease of application, cost-effectiveness, remarkable adsorption material recovery rates, and its adaptability to a wide array of waste materials sourced from other sectors.

Within the realm of adsorption, zeolite emerges as a remarkable candidate. Zeolite is a geologically derived material characterized by its intricate crystalline structure replete with a multitude of porous channels. These attributes grant zeolite exceptional adsorption and ion

exchange capacities, rendering it highly suitable for the removal of heavy metals from aqueous environments. Nonetheless, a critical challenge associated with zeolite-based adsorption lies in the efficient recovery and reusability of the adsorbent material. To address this predicament, extensive efforts have been directed towards the exploration of polymer compounds extracted from waste sources and various biological materials. These have been ingeniously integrated with zeolite, taking the form of fibers, granules, membranes, and other configurations. This amalgamation, denoted as “polymer–zeolite”, offers the promise of efficacious heavy metal removal, coupled with facile recycling and cost-effective implementation.⁵

Furthermore, cellulose acetate, a material derived from abundant waste sources, such as sugarcane bagasse, has garnered significant attention. This biopolymer exhibits noteworthy potential as a formidable component in the polymer–zeolite composite, further emphasizing its prominence in the pursuit of efficient heavy metal removal strategies.⁶

Building upon the successes of prior research endeavors that have harnessed the synergy between zeolite and cellulose acetate for the removal of heavy metals from aqueous solutions,⁶⁻⁹ this study embarks on a quest to explore the preparation of cellulose acetate derived from bagasse for the production of cellulose acetate/zeolite fibers. The primary aim of this investigation is to harness these fibers for the adsorption of Pb^{2+} and Cu^{2+} from aqueous solutions. In addition to its immediate practical implications, this research also aligns itself with the broader objectives of mitigating agricultural waste and promoting environmentally friendly methodologies for heavy metal removal. Consequently, this study not only offers potential solutions to the pressing issue of heavy metal pollution, but also contributes to a more sustainable and ecologically conscious approach to waste utilization and management.

EXPERIMENTAL

Chemicals and reagents

Zeolite A-3, with the chemical formula of $MeO.Al_2O_3.mSiO_2.nH_2O$ and a particle size of 200 mesh, was procured from Spectrum Chemicals and Laboratory Products Co., Ltd., Japan. Sodium hydroxide, nitric acid, sulfuric acid, acetone, acetic acid, and hydrochloric acid were sourced from Xilong

Scientific Co. Ltd., China, while acetic anhydride was acquired from Scharlab S.L., Spain.

Solutions of Cu^{2+} and Pb^{2+} ions were meticulously prepared by dissolving precisely weighed quantities of $CuSO_4.5H_2O$ from Sci-Tech Co. Ltd., China, and $Pb(NO_3)_2$ from Fenxi Chun Chiji, China. Throughout the experimental process, analytical-grade chemicals were exclusively employed, and the solutions were meticulously prepared using deionized water. The solutions containing Pb^{2+} and Cu^{2+} contaminants at specific concentrations were methodically generated within the confines of our laboratory.

Zeolite/cellulose acetate fiber production

Preparation of SCB and synthesis of cellulose

Raw material

Sugarcane bagasse (SCB) was washed several times after being squeezed and dried in the sun for several hours. Finally, SCB was dried in the oven at 50 °C for 24 hours, as seen Figure 1.

Alkaline pretreatment

Alkaline treatment was conducted on 12 g of SCB treated in the stage above, placed into 500 mL of distilled water. The sample was filtered and put in 100.0 mL of NaOH (0.25 M) after 24 h. Then, the mixture underwent vacuum filtration and washing with distilled water to remove NaOH (Fig. 2).

Cellulose extraction

After treating with NaOH, SCB was introduced into a two-necked flask and refluxed with a mixture of ethanol and HNO_3 4:1 (v/v), which was replaced after each hour in 3 hours. After reflux, the bagasse mixture was filtered by vacuum filtration and washed with distilled water to remove the acid. From the amount of bagasse obtained from the above process, cellulose was extracted successfully. The cellulose obtained was further dried at 105 °C in the oven for 3 hours to prepare for the next step (Fig. 3).

Preparation of cellulose acetate (CA)

There are two synthesis ways of cellulose acetate – cellulose triacetate and cellulose diacetate, which are CA derivatives as a function of CH_3CO , as can be observed in Figure 4. In this study, cellulose diacetate was produced, following the method of Chen *et al.*⁷

Preparation of cellulose triacetate (CTA)

At room temperature, 2.000 g of SCB cellulose was mixed with 50 mL of 36% acetic acid under magnetic stirring in a 250 mL Erlenmeyer flask. After stirring for 30 min, 0.16 mL of 98% H_2SO_4 and 18 mL of acetic acid were poured into the flask and continuously stirred for 25 min before filtering with 64 mL acetic anhydride. The filtrated solution was then continuously stirred around 15 min and then left overnight (16-24 h) at room temperature. The solution was vacuum filtered with water to form cellulose triacetate (CTA), which

was then washed three times and dried at 70 °C for two



Figure 1: Sugarcane bagasse

hours.



Figure 2: Alkaline treatment of SCB



Figure 3: Refluxed SCB (left) and cellulose (right)

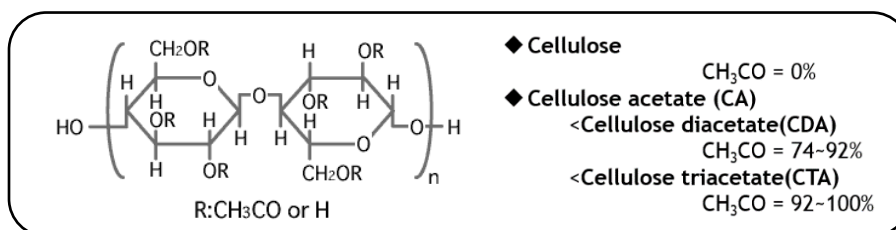


Figure 4: Cellulose acetate derivatives

Preparation of cellulose diacetate (CDA)

Cellulose diacetate (CDA) was prepared according to the method described by Chen *et al.* (2015),⁷ in the following manner. Initially, a 250 mL Erlenmeyer flask was employed to dissolve 2.000 g of CTA in 40.00 mL of CH₃COOH. Subsequently, 1.50 mL of 0.25 M H₂SO₄ and 4.40 mL of distilled H₂O were added to the flask. The resulting mixture was heated using a reflux system at 80 °C. Following a 10-minute heating period, the suspension was filtered through a glass fritted funnel to eliminate insoluble particles. The obtained solution was then subjected to dropwise addition of distilled water to induce the formation of CDA. The resulting precipitate was subsequently filtered, washed three times with water, and dried at 50 °C for 2 hours in an oven.

Production of acetate/zeolite (CA/Ze) fiber

Cellulose acetate (6,000 g) was dissolved in a solvent mixture of acetone and water in a 1:6 weight

ratio, employing agitation through stirring over a duration of 3 hours. Subsequently, gradual addition of 1.5 grams of zeolite was incorporated into the aforementioned system, which was then stirred for an additional 3 hours at room temperature. Following the mixing process, fibers were fabricated utilizing both dry spinning and wet spinning techniques, as depicted in Figure 5.

Characterization of cellulose acetate/zeolite (CA/Ze) fiber

Fourier transform infrared (FTIR) spectroscopy

The IR spectra for all the samples were acquired using an FTIR spectrometer (Shimadzu Prestige 21) set at a resolution of 4 cm⁻¹, comprising 28 scans for each spectrum, utilizing KBr tablets at a weight ratio of 1:100. These analyses were performed at the laboratory of Biosustainable Environmental Engineering within the Faculty of Science and

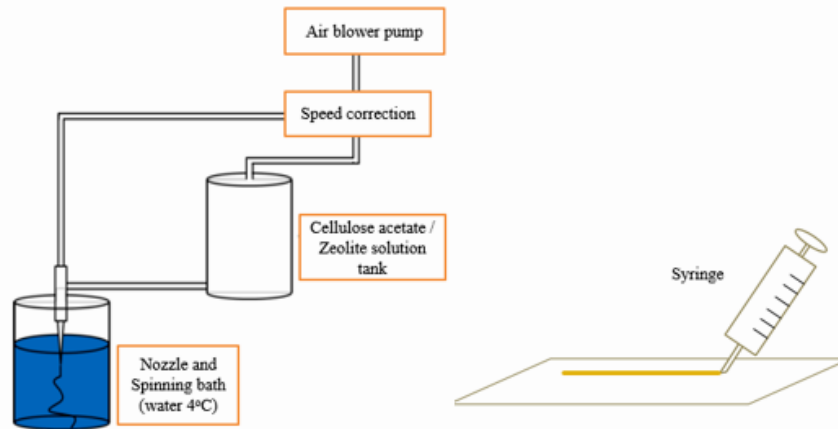


Figure 5: Wet spinning system (left) and dry spinning system (right)

Scanning electron microscopy (SEM)

SC-701MC Quick Cool Coater (Sanyu Denshi Co., Ltd.) equipment and a Jeol JSM-5300LV, at and 30 kV, were used to conduct morphological analysis (surface and cross-sections) of the prepared samples. Cross-section micrographs were obtained for samples fractured in liquid nitrogen.

Hydration ability of CA/Ze fiber

The CA/Ze hydration ability test was performed by weighing the dry fiber with the specified mass. The CA/Ze fiber was then immersed in water and the fiber mass was reassessed continuously with regular intervals from 1 hour to 9 hours, and then after 14, 19, and 24 hours. The hydration ability of the composite fiber was calculated as follows:

$$SC (\%) = \frac{m - m_0}{m_0} \times 100\% \quad (1)$$

where SC – hydration ability of CA/Ze fibers (%), m_0 – initial mass of CA/Ze fibers (g), m – weight of CA/Ze fibers after a period of time (g).

Adsorption experiments of heavy metal ions

CA/Ze fiber was added to Pb^{2+} and Cu^{2+} heavy metal solution. Experiments were conducted to determine the optimal conditions of the treatment, including pH, reaction time, input heavy metal concentration, CA/Ze fiber mass and fiber reuse capacity CA/Ze.

The number of metal ions adsorbed on an adsorption unit at time t (min) and equilibrium time was calculated by the relation:

$$q = (C_0 - C) \times \frac{V}{m} \quad (2)$$

where q (mg/g) – amount of heavy metals adsorbed per unit of fiber mass (adsorption capacity), C_0 (mg/L) – concentration of metal ions initially, C (mg/L) – concentration of metal ions after adsorption, V (L) – volume of the solution, m (g) – mass of CA/Z fiber.

The following formula was used to calculate adsorption efficiency:

$$\%H = \left(\frac{C_0 - C_t}{C_0} \right) \times 100\% \quad (3)$$

where C_0 (mg/L) – concentration of heavy metal in the initial solution, C_t (mg/L) – concentration of heavy metal after adsorption, $\%H$ (%) – adsorption efficiency of CA/Ze fibers.

Regeneration ability of CA/Ze fiber

After the adsorption experiments, the CA/Ze fibers were collected and subsequently added to a 0.1M HCl solution. The mixture was shaken at a speed of 150 revolutions per minute (rpm) for a duration of 8 hours, maintaining room temperature conditions. Subsequently, the fibers were rinsed with distilled water and air-dried at room temperature to enable their reuse.

To assess the regeneration of CA/Ze fibers, the previously treated fibers were placed in an Erlenmeyer flask containing 50 mL of solutions containing Pb^{2+} and Cu^{2+} ions at an optimal pH. The concentrations of the metal ions in the solutions were 25 mg/L each. The Erlenmeyer flask was then subjected to shaking at a speed of 150 rpm for a duration of 150 minutes at room temperature. Following this, the CA/Ze fibers were separated from the solutions, and the concentration of heavy metal ions was measured to assess the treatment efficiency of the regenerated fibers.

RESULTS AND DISCUSSION

Characteristic properties of cellulose acetate/zeolite (CA/Ze) fibers

Synthesis of cellulose acetate from SCB

The synthesis of cellulose acetate involved a multi-step process starting with SCB purification. Cellulose was then extracted and acetylated to form cellulose triacetate (CTA) by introducing acetyl groups. Subsequently, the deacetylation of CTA was conducted to reduce the acetyl

functional groups ($\text{CH}_3\text{CO}-$) in the structure, resulting in the production of cellulose acetate (CA) as presented in Figure 6. This was clearly demonstrated by the comparative FTIR spectra of CTA and CA in Figure 7. The deacetylation process had 53% efficiency (Table 1). CTA reacted with acetic acid and sulfuric acid, and, after deacidification, was reacted with water to obtain the precipitate – cellulose acetate.

Fourier transform infrared (FTIR) spectroscopy

Figure 7 illustrates the Fourier transform infrared (FTIR) spectra of SCB and cellulose, revealing the removal of lignin from SCB based on the observed peaks at 1605 and 1517 cm^{-1} . The increased transmittance indicates a reduction in the $\text{C}=\text{O}$ bond of lignin, while the intensified transmittance at 1164 cm^{-1} , characteristic of arabinoxylans and that at 1509 cm^{-1} , associated with hexenuronic acids in the hemicellulose structure, which confirms the elimination of significant amounts of hemicelluloses. Additionally, changes in the FTIR spectra of bagasse and cellulose at 3429 cm^{-1} and 2914 cm^{-1} indicate an increase in OH bonding and the characteristic CH bonding of the cellulose molecule, consistent with previous findings by Chen *et al.* (2015).⁷

The FTIR spectra of cellulose and CTA demonstrate alterations in the peak patterns,

which reflect successful acetylation, a reduction in the number of OH groups in the cellulose structure, and an increase in acetylsalicylated $\text{CH}_3\text{CO}-$ groups in cellulose triacetate. The decrease in the peaks of CTA and cellulose at the wavelength of 3400 cm^{-1} confirms the replacement of OH groups by acetyl groups in the CTA structure. This replacement is indicated by the presence of $\text{C}=\text{O}$ bonds from the carbonyl ester, as well as $\text{C}-\text{H}$ and $\text{C}-\text{O}$ bonds (cellulose linker and acetyl group) at 1750 , 1360 , and 1220 cm^{-1} . Notably, the FTIR spectra of CA and CTA exhibit changes at wavelengths of 3400 , 1750 , 1237 , and 1047 cm^{-1} , corresponding to the vibrations of OH, $\text{C}=\text{O}$, $\text{C}-\text{C}-\text{O}$, and $\text{C}-\text{O}$ groups, in agreement with the findings of Chen *et al.*⁷ These changes reflect the successful deacetylation process, where some acetyl groups of CTA are replaced by OH groups in the CA structure. The structural comparison between the synthesized CA/Ze fibers and the reference structures of cellulose acetate (CA) and zeolite, as depicted in Table 2, revealed striking similarities in characteristic peaks, resembling the functional groups present in Zeolite and CA. This observation suggests a covering of the zeolite by the fiber, establishing a bonding interaction between the zeolite and the cellulose acetate within the CA/Ze fiber structure.

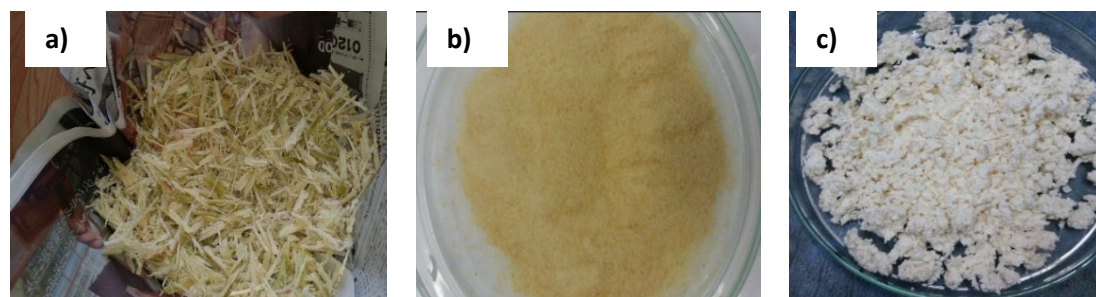


Figure 6: (a) Sugarcane bagasse, (b) cellulose triacetate (CA) and (c) cellulose acetate (CA)

Table 1
Mass yield results of each stage

Process	Input mass (g)	Obtained mass (g)	Yield (%)
SCB → Cellulose	12	6.2	52
Cellulose → CTA	6.2	7.7	124
CTA → CA	7.7	4.1	53
SCB → CA	12	4.1	34

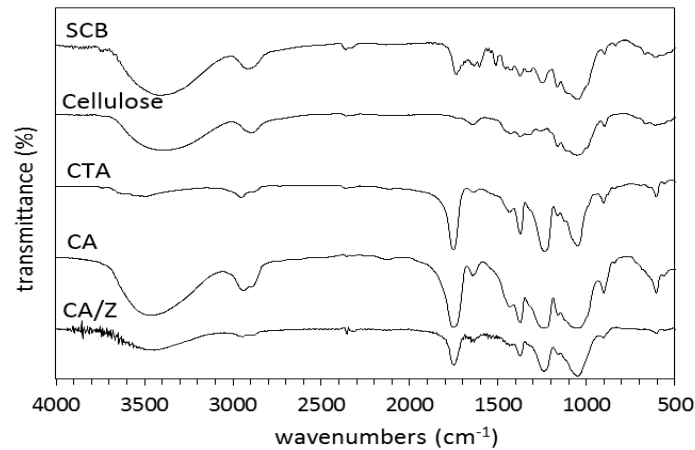


Figure 7: FTIR spectra of SCB, cellulose, CTA, CA and CA/Ze structures

Table 2
Structure of CA material and CA/Ze fiber⁷

Functional groups	Wavelength (cm ⁻¹)	
	CA material	Zeolite
O-H	3400	3478, 3495
C-O	1047	-
C=O	1750	-
C-C-O	1237	-
β(1-4)	900	-
Si-O-Si	-	1209
Si-O, Al-O	-	1087, 1064
Si-O-H, Al-O-H	-	920

Scanning electron microscopy (SEM)

The SEM images of the CA/Ze fibers are presented in Figure 8 (surface view) and Figure 9 (cross-section view). Upon observing Figure 8, it is evident that the fiber surface exhibits a densely packed structure, adorned with numerous small particles adhering to the surface of the CA/Ze fiber. These particles are identified as zeolites, which form a covering layer on the material surface. Figure 9 provides a cross-sectional view, revealing the stable and compact nature of the CA/Ze fiber. This observation further elucidates the incorporation of zeolite and CA within the fiber structure.

Hydration ability of CA/Ze fiber

The hydration capacity of CA/Ze fiber (SC%) signifies its capacity to imbibe water, thus influencing the fiber’s stability and its efficacy in sequestering heavy metal ions in aqueous solutions. As depicted in Figure 10, the hydration capacity of CA/Ze fibers exhibits a time-dependent increase, primarily within the initial hour, followed by a marginal increase until

saturation is attained by the sixth hour. The hydrophilicity of cellulose acetate elucidates the underlying mechanism responsible for the water retention capabilities of CA/Ze fibers. Notably, after 24 hours, the fibers’ hydration level reaches approximately 70% and remains consistently sustained, indicative of their favorable mechanical stability in water and their potential for employment in metal treatment experiments involving aqueous solutions.

Adsorption experiments of heavy metal ions
Factors affecting the adsorption process

The adsorption process undergoes substantial modulation due to the concentration of H⁺ and OH⁻ ions within the solution, signifying the pivotal significance of pH value as a determinant factor necessitating meticulous investigation and control. These ions possess the capability to adhere to the adsorption sites on the surface of the adsorbent, thereby altering their behavior and affinity for the analyte. The pH level of water significantly impacts the adsorption capacity of CA/Ze fiber by influencing the presence of metal ions. Analysis of Figure 11 reveals that the CA/Ze

fiber material exhibits the highest adsorption capacity for Pb^{2+} at a pH of 5, followed by Cu^{2+} , with adsorption capacities of 14.07 mg/g and 5.50 mg/g, respectively.

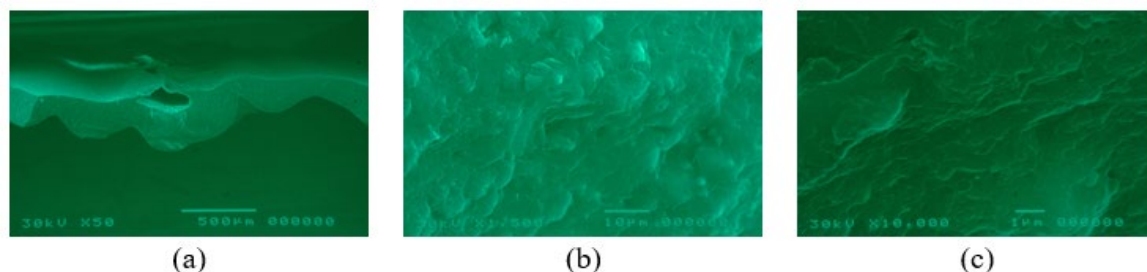


Figure 8: SEM images of CA/Ze fiber surfaces in contact with air, at different magnifications (a) x50, (b) x1,500 and (c) x10,000

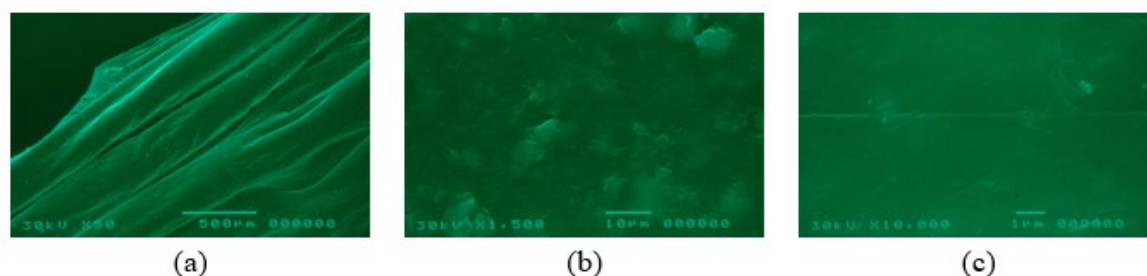


Figure 9: Cross-sections of CA/Ze fiber at different magnifications magnifications (a) x50, (b) x1,500 and (c) x10,000

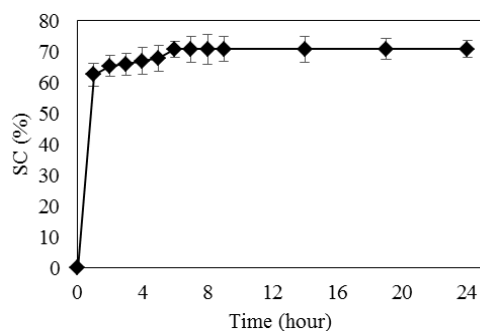


Figure 10: Hydration ability of CA/Ze fiber

This propensity arises from the negatively charged surface of CA/Ze, enabling the absorption of lead and copper ions. At lower pH levels, characterized by strong acidity in water and enhanced affinity of hydrogen ions (H^+) over Cu^{2+} or Pb^{2+} ions, a competitive relationship arises between them, thereby diminishing the material's performance.

Conversely, a pH value exceeding 5 renders the surface charge of the material more positive, thereby diminishing its lead adsorption ability. This observation aligns with previous studies,

highlighting higher lead adsorption by the zeolite at pH 5.

Conversely, at pH 5, the ionization of zeolite's hydroxyl groups (Si-OH and Al-OH) facilitates the adsorption of Cu^{2+} or Pb^{2+} ions in water. The efficacy of CA/Ze fibers is notably influenced by the adsorption time. Prolonged adsorption durations increase the exposure of the material to metal ions, enhancing the process efficiency and the adsorption capacity due to augmented surface area accessibility for adsorption. However, an extended duration beyond a certain threshold

diminishes the available active area on the adsorbent, leading to a gradual decline in the adsorption rate. As depicted in Figure 12, the optimum duration for Pb^{2+} adsorption is determined to be 150 minutes, whereas for Cu^{2+} , it extends to 180 minutes, with respective adsorption capacities for Pb^{2+} of 13.9 mg/g and for Cu^{2+} of 3.5 mg/g.

The exchange of Pb^{2+} and Cu^{2+} metal ions with zeolite particles on and within the CA/Ze material structure serves to balance the ionic concentration in the solution. Figure 13 illustrates that the handling capacity of the CA/Ze material for Pb^{2+} and Cu^{2+} metal ions decreases with increasing initial concentrations of these ions. For Pb^{2+} , the maximum treatment concentration is less than 25 mg/L, achieving a performance of approximately 98%. For Cu^{2+} , the peak performance of CA/Ze fibers is evident at concentrations lower than 10 mg/L, showcasing a remarkable processing efficiency of 91.7%. This phenomenon may stem from the observation that lower concentrations yield a higher abundance of available adsorption sites, whereas higher concentrations result in a reduction of these sites. With an escalation in the concentrations of Pb^{2+} and Cu^{2+} , the adsorption

sites on the adsorbent gradually reach saturation, becoming entirely occupied by higher concentrations of Pb^{2+} and Cu^{2+} . Consequently, the capacity to adsorb further Pb^{2+} and Cu^{2+} from the solution diminishes rapidly, leading to a notable decline in the adsorption potential.¹³

The examination of the recyclability of the CA/Ze material demonstrates its potential for reuse, which represents a significant advantage of adsorbent materials. Compared to normal zeolite powder, the CA/Ze fibers can be easily separated from the solution containing heavy metal ions after treatment. The recovery test of the CA/Ze material was conducted with three replicates, revealing that the metal ion adsorption efficiency of the material decreases after three regeneration cycles. The adsorption capacity of the regenerated CA/Ze material for Pb^{2+} and Cu^{2+} ions is 1.109 mg/g and 0.448 mg/g, respectively (Fig. 14). This decrease can be attributed to the strong binding of some metal ions to the material structure during ion adsorption and exchange. Consequently, the recycling process of the CA/Ze material cannot completely deplete these ions, leading to a gradual reduction in the handling efficiency of heavy metals with each subsequent reuse.

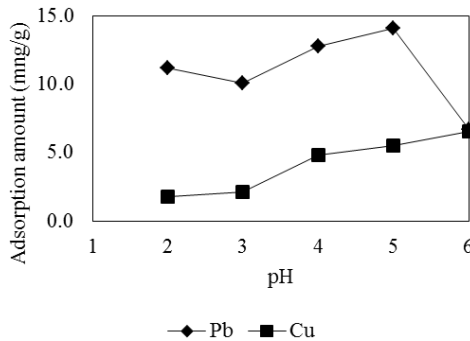


Figure 11: Effect of pH on adsorption of metal ions onto CA/Ze fibers

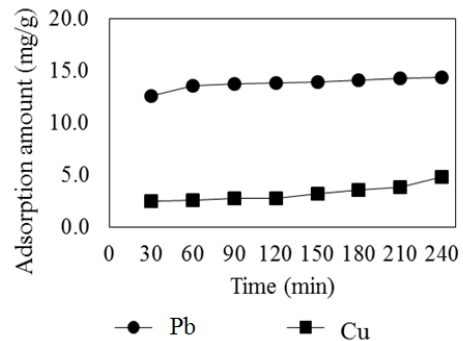


Figure 12: Effect of process time on adsorption of metal ions onto CA/Ze fibers

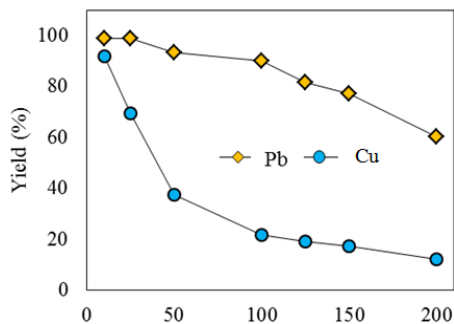


Figure 13: Effect of initial metal ions concentration on adsorption onto CA/Ze fibers

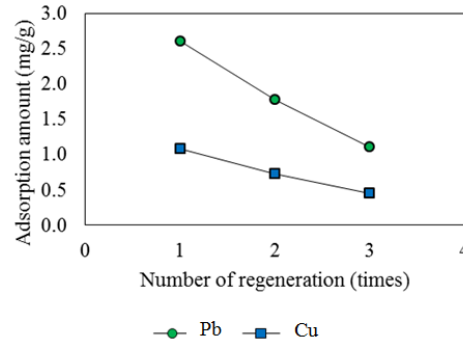


Figure 14: Recovery of the adsorption ability of CA/Ze fibers after three adsorption cycles

Langmuir and Freundlich isothermal models

The adsorption isotherms were investigated using the Langmuir and Freundlich isothermal equations, and the respective parameters are presented in Table 3. The Freundlich model exhibited lower suitability than the Langmuir model, indicating that the Langmuir isothermal model better explains the CA/Ze test results in this study (Figs. 15 and 16).

In the Langmuir model, the maximum adsorption capacities (q_m) of Pb^{2+} and Cu^{2+} are 20.576 and 3.273 mg/g, respectively. Furthermore, the Langmuir adsorption constants (K_L) of Pb^{2+} and Cu^{2+} are 0.315 and 0.121, respectively. Moreover, the results suggest that both physical and chemical mechanisms contribute to the absorption of Pb^{2+} and Cu^{2+} by CA/Ze.

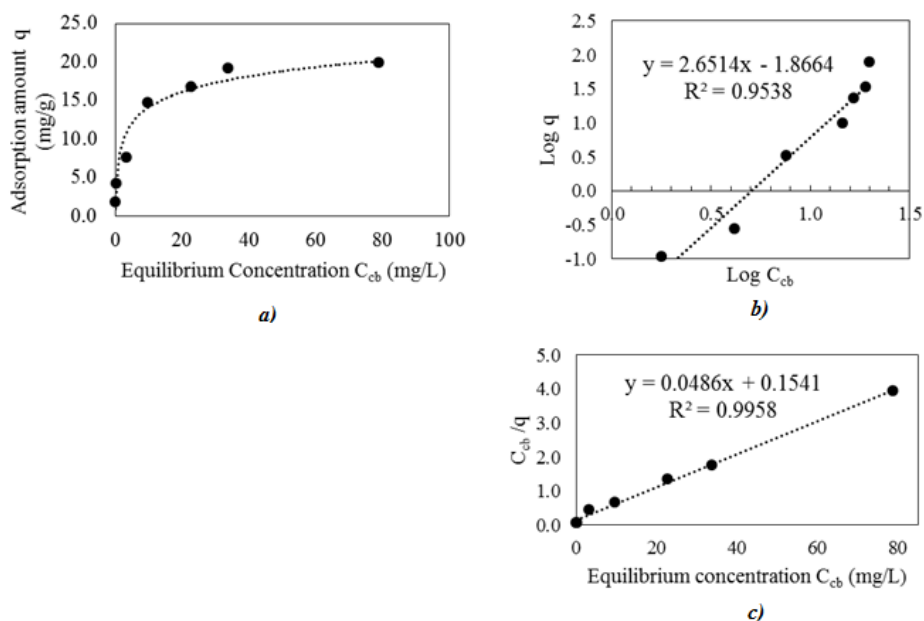


Figure 15: Adsorption isotherm of Pb^{2+} ions ($m = 0.3$ g, $V = 50$ mL, $pH = 5$, shaking time: 150 min), a) Isothermal adsorption curve, b) Freundlich isothermal line and c) Langmuir isothermal line

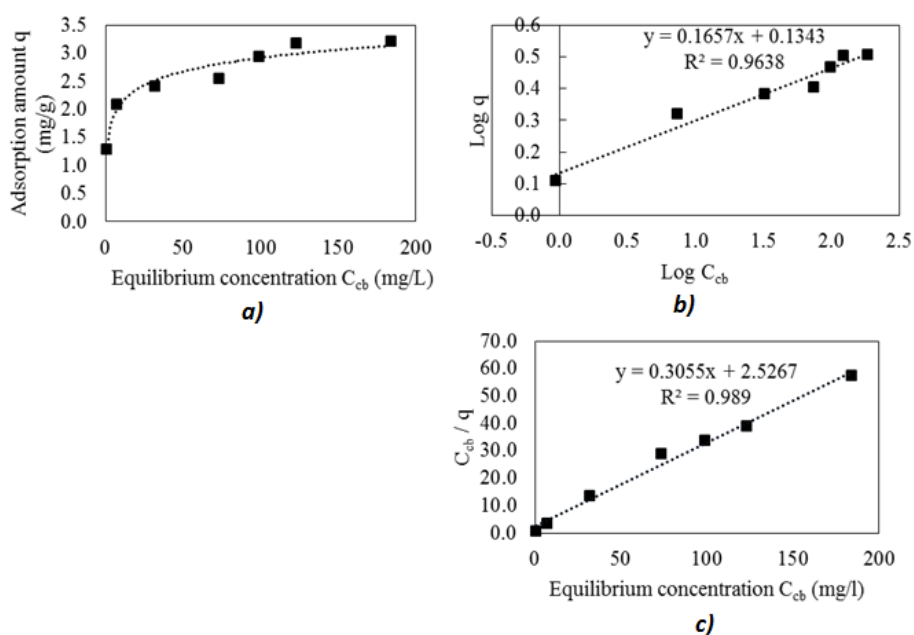


Figure 16: Adsorption isotherm of Cu^{2+} ions ($m = 0.3$ g, $V = 50$ mL, $pH = 5$, shaking time: 150 min), a) Isothermal adsorption curve, b) Freundlich isothermal line and c) Langmuir isothermal line

Table 3
Langmuir and Freundlich isotherm parameters and correlation coefficients for Pb²⁺ and Cu²⁺ adsorption onto CA/Ze fiber

Isotherm models		Metals	
		Pb ²⁺	Cu ²⁺
Langmuir	q _m	20.576	3.273
	K _L	0.315	0.121
	R ²	0.996	0.989
Freundlich	K _f	0.014	1,362
	1/n	2.651	0.166
	R ²	0.954	0.964

Table 4
Summary of cellulose-based adsorption studies utilizing the Langmuir isothermal model for Cu²⁺ and Pb²⁺ removal

Materials	Adsorbate	Optimum pH or range	Adsorption capacity (mg/g)	Study
Carboxymethyl cellulose	Pb	1	25.9	12
Zwitterionic cellulose acetate/graphene oxide	Cu	6	32	13
Thiol-functionalized cellulose	Cu	4	49	14
	Pb		22	
Cellulose nanocrystal	Pb	6	6.4	15
		4	3.5	
		5	10.5	16
Cellulose-based composite membrane (12 layers)	Cu	6	17.3	
			23	17
			25	
Cellulose acetate/titanium oxide (TiO ₂)	Cu	5.2-5.8	23	17
	Pb		25	
CA/Ze	Cu	4-6	4.8	Present study
	Pb		14.3	

However, chemical adsorption predominantly occurs through monolayer adsorption, as supported by the results in Table 3. The maximum adsorption capacities of CA/Ze are arranged in the order of Pb²⁺ > Cu²⁺, with Pb²⁺ displaying the highest adsorption capacity and Langmuir constant. These findings indicate that the adsorption behavior of heavy metal ions remains consistent, even after combining zeolite powder with the CA carrier.

Table 4 provides a comprehensive overview of the adsorption capacities exhibited by various cellulose-based adsorbents in the removal of copper and lead ions. These capacities have been assessed under largely consistent experimental conditions for the respective adsorbents. The documented values denote monolayer adsorption capacities falling within a range that aligns with those reported by several other researchers conducting similar studies. This congruence in findings establishes a valuable benchmark for comparative analysis with the results obtained in the current study.

CONCLUSION

This study has successfully developed cellulose acetate (CA)/zeolite fibers as a promising and environmentally friendly solution for effectively removing Pb²⁺ and Cu²⁺ ions from aqueous solutions. The utilization of zeolite's exceptional adsorption capacity and cellulose acetate derived from waste biomass sources presents a compelling strategy to combat heavy metal pollution. Characterization results unequivocally demonstrate the successful integration of zeolite particles into the CA fibers, enhancing their adsorption potential. The adsorption experiments substantiate the superior performance of the CA/zeolite fibers, with optimized conditions for pH, reaction time, initial metal ion concentration, and fiber mass established. These fibers exhibit noteworthy adsorption capacities for Pb²⁺ and Cu²⁺ ions.

While the recyclability of the CA/zeolite fibers has been demonstrated, the adsorption capacity experiences a decline with each successive regeneration cycle due to the strong binding between metal ions and the material

structure. Further investigation is necessary to optimize the regeneration process. The Langmuir isotherm model offers a superior fit to the experimental data, suggesting monolayer adsorption, involving both physical and chemical mechanisms. The maximum adsorption capacities of these fibers contribute to the expanding knowledge base on sustainable materials for water treatment, emphasizing the significance of addressing heavy metal pollution, while advocating for waste utilization and effective management practices.

REFERENCES

- ¹ T. T. C. Truong, K. Takaomi and H. M. Bui, *J. Serb. Chem. Soc.*, **84**, 83 (2019), <https://doi.org/10.2298/JSC180606085T>
- ² Z. Xu, Q. Zhang, X. Li and X. Huang, *Chem. Eng. J.*, **429**, 131688 (2022), <https://doi.org/10.1016/j.cej.2021.131688>
- ³ T. A. Saleh, M. Mustaqeem and M. Khaled, *Environ. Nanotechnol. Monit. Manag.*, **17**, 100617 (2022), <https://doi.org/10.1016/j.enmm.2021.100617>
- ⁴ H. Xiang, X. Min, C. J. Tang, M. Sillanpää and F. Zhao, *J. Water Process. Eng.*, **49**, 103023 (2022), <https://doi.org/10.1016/j.jwpe.2022.103023>
- ⁵ M. F. Mubarak, A. M. G. Mohamed, M. Keshawy, T. A. elMoghny and N. Shehata, *Alex. Eng. J.*, **61**, 4189 (2022), <https://doi.org/10.1016/j.aej.2021.09.041>
- ⁶ K. I. Kinoti, J. Ogunah, C. M. Muturia and J. M. Marangu, *J. Chem.*, **2022**, 4250299 (2022), <https://doi.org/10.1155/2022/4250299>
- ⁷ X. Chen, *Information*, **6**, 14 (2015), <https://doi.org/10.3390/info6010014>
- ⁸ Y. Wang, F. Lin and W. Pang, *J. Hazard. Mater.*, **160**, 371 (2008), <https://doi.org/10.1016/j.jhazmat.2008.03.006>
- ⁹ P. Praipipat, P. Ngamsurach and N. Roopkhan, *Sci. Rep.*, **13**, 1873 (2023), <https://doi.org/10.1038/s41598-023-29055-4>
- ¹⁰ S. Jangkorn, S. Youngme and P. Praipipat, *Heliyon*, **8**, e09323 (2022), <https://doi.org/10.1016/j.heliyon.2022.e09323>
- ¹¹ M. M. Lakouraj, F. Mojerlou and E. N. Zare, *Carbohydr. Polym.*, **106**, 34 (2014), <https://doi.org/10.1016/j.carbpol.2014.01.092>
- ¹² L. M. Furtado, D. P. Fuentes, R. A. Ando, P. V. Oliveira and D. F. Petri, *J. Clean. Prod.*, **380**, 134969 (2022), <https://doi.org/10.1016/j.jclepro.2022.134969>
- ¹³ H. Huang, Y. Shen, J. Yu and H. Guo, *BioResources*, **13**, 3642 (2018), <https://doi.org/10.15376/biores.13.2.3642-3658>
- ¹⁴ H. Y. Choi, J. H. Bae, Y. Hasegawa, S. An, I. S. Kim *et al.*, *Carbohydr. Polym.*, **234**, 115881 (2020), <https://doi.org/10.1016/j.carbpol.2020.115881>
- ¹⁵ C. V. Abiazim, A. B. Williams, A. I. Inegbenebor and C. T. Onword, *J. Phys. Conf. Ser.*, **1299**, 012122 (2019), <https://doi.org/10.1088/1742-6596/1299/1/012122>
- ¹⁶ X. Pei, L. Gan, Z. Tong and H. Gao, *J. Hazard. Mater.*, **406**, 124746 (2021), <https://doi.org/10.1016/j.jhazmat.2020.124746>
- ¹⁷ K. A. Gebru and C. Das, *J. Water Process. Eng.*, **16**, 1 (2017), <https://doi.org/10.1016/j.jwpe.2016.11.008>